Ultrasonics 83 (2018) 179–187

Contents lists available at ScienceDirect

Ultrasonics

journal homepage: www.elsevier.com/locate/ultras

Sonochemical growth of nanomaterials in carbon nanotube

M. Jesionek [a,*], M. Nowak [a], K. Mistewicz [a], M. Kępińska [a], D. Stróż [b], I. Bednarczyk [c], R. Paszkiewicz [d]

[a] Institute of Physics – Centre for Science and Education, Silesian University of Technology, Krasińskiego 8,40-019 Katowice, Poland
[b] Institute of Material Science, University of Silesia, 75 Pułku Piechoty 1A, 41-500 Chorzów, Poland
[c] Faculty of Materials Science, Silesian University of Technology, Krasińskiego 8, 40-019 Katowice, Poland
[d] Division of Microelectronics and Nanotechnology, Wrocław University of Technology, Długa 65, 53-633 Wrocław, Poland

ARTICLE INFO

Article history:
Received 19 December 2016
Received in revised form 6 March 2017
Accepted 16 March 2017
Available online 18 March 2017

Keywords:
Carbon nanotubes
Antimony sulfoiodide (SbSI)
Antimony selenoiodide (SbSeI)
Sonochemistry
Encapsulation
Ultrasonic joining

ABSTRACT

Recent achievements in investigations of carbon nanotubes (CNTs) filled with ternary chalcohalides (antimony sulfoiodide (SbSI) and antimony selenoiodide (SbSeI)) are presented. Parameters of sonochemical encapsulation of nanocrystalline semiconducting ferroelectric SbSI-type materials in CNTs are reported. This low temperature technology is convenient, fast, efficient and environmentally friendly route for producing novel type of hybrid materials useful for nanodevices. Structure as well as optical and electrical properties of SbSI@CNTs and SbSeI@CNTs are described. Advantages of ultrasonic joining of such filled CNTs with metal microelectrodes are emphasized. The possible applications of these nanomaterials as gas sensors are shown.

1. Introduction

Carbon nanotubes (CNTs), discovered by Iijima [1], have various potential applications as: sensors, field emission displays, semiconductor nanodevices and hydrogen storage media. There is a great demand for control versatile electronic characteristics of CNTs. One strategy is to use the CNTs themselves, controlling useful properties *via* their radii and morphologies. An alternative approach leading to new features of CNTs is based on filling them with condensed substances from a wide range of materials [2–6], including 1D crystals of metals, metal salts and oxides, semiconductors, superconductors, and chains of fullerene or endofullerene molecules. Such objects are distinguished in their physical and chemical properties from both hollow nanotubes and the encapsulated substances. There are a few methods of filling CNTs with different substances: catalytic synthesis of nanotubes using metals as catalysts [3], capillary drawing-in of molten materials or materials dissolved in solvents having a low surface tension [4], saturation with metal vapor [5], electrochemical methods based on passing the electrical current through an electrolyte containing dissolved metal atoms [6], and sonochemistry [7,8].

It is well known [9–14] that powerful ultrasound evoking cavitation can induce new reactivity leading to the formation of unexpected chemical species. The application of sonochemistry to fill CNTs is also justified by the fact that ultrasonication is often used to cut the outer caps of CNTs [15].

Among materials encapsulated within CNTs are elements (e.g., Bi, Sb, S, Se, Te, I_2), halogenides (e.g., BaI_2, NaCl, AgBr), oxides (e.g., Sb_2O_3), and chalcogenides (e.g., Sb_2S_3, CdS, SnSe, SnTe, HgTe), too [5,6]. Recently, CNTs have been filled with ternary compounds formed from the group 15–16–17 elements, i.e. antimony sulfoiodide (SbSI) [7] and antimony selenoiodide (SbSeI) [8]. It should be noted that SbSI is semiconducting ferroelectric with the indirect forbidden energy band gap $E_{glf} = 1.829(27)$ eV [16] and $T_c = 292(1)$ K Curie temperature [17]. SbSI is one of the best piezoelectric crystals with high piezoelectric modulus $d_v = 1 \cdot 10^{-9}$ C/N [5], extremely large electromechanical coupling coefficient $k_{33} = 0.9$ [18], and high electrostrictive constant $Q_{3333} = 4.6(1) \cdot 10^{-13}$ m^2/V^2 [19]. An unusually large number of very attractive and suitable phenomena are observed in SbSI-type materials, e.g., photoferroelectric, pyroelectric, pyrooptic, piezoelectric, electromechanical, electrooptic, photorefractive, photocatalytic, and nonlinear optical effects. Therefore SbSI-type materials are considered to be important for many applications (see the literature cited in [16,17,19]).

The aim of this paper is to present recent achievements in using ultrasounds for encapsulation of SbSI-type materials in CNTs as well as for fabrication of electrical gas nanosensors. Such sensors need reliable, secure, long-lasting bonds between filled CNTs and electrodes. In this work ultrasonic processing is used

* Corresponding author.
E-mail address: Marcin.Jesionek@polsl.pl (M. Jesionek).

http://dx.doi.org/10.1016/j.ultras.2017.03.014
0041-624X/

for nanojoining of SbSI@CNTs and SbSeI@CNTs with metal microelectrodes for the first time. The fabricated structures have been successfully applied to sense carbon dioxide.

2. Experiment

SbSI and SbSeI were prepared in CNTs ultrasonically from elements (Sb, I_2, and S or Se). Methanol and/or ethanol served as solvents for these reactions. Antimony (99.95%), selenium (99.5%) and multi–walled CNTs (659258–10G, 90+%) were purchased from Sigma–Aldrich (USA). Sublimated sulfur, iodine, absolute methanol, and absolute ethanol were of analytical purity (Avantor Performance Materials, Poland). In a typical procedure of SbSI@CNTs fabrication, the mixture with stoichiometric ratio of e.g. 0.380 g Sb, 0.099 g S and 0.394 g I_2, was immersed with 0.282 g of CNTs in 40 ml of alcohol. The fabrication of SbSeI@CNTs was performed for four times greater amount of Se in comparison with stoichiometric ratio. It allowed to avoid excess formation of SbI_3. For example, 0.156 g Sb, 0.404 g Se and 0.165 g I_2, were immersed with 0.102 g of CNTs in 10 ml of alcohol.

The reagents were contained in closed 54 ml Pyrex glass cylinders of 20 mm inside diameter and 1 mm thickness. The cylinders were partly submerged in water in cup-horn of ultrasonic reactor biased with VCX-750 ultrasonic processor with sealed converter VC-334 (Sonics & Materials, Inc., USA). The used ultrasounds had the frequency of 20 kHz and 565 W/cm^2 power density guaranteed by the manufacturer. The cup-horn was filled with water continuously pumped through refrigerated circulating bath AD07R (PolyScience, USA). The sonolysis was carried out for 3 h at 323 K temperature. The color of the suspension changed gradually indicating the growth process of SbSI and SbSeI. To control this process, measurements of optical diffusive reflectance $R_d(\lambda)$ were performed using spectrophotometer PC2000 equipped with integrating sphere ISP-REF (Ocean Optics Inc., USA). The standard WS-1 (Ocean Optics Inc., USA) was used as a reference. It was assumed that the sonochemical process is finished, when the spectral characteristics of $R_d(\lambda)$ do not change with time. At the end, brown-purple SbSI@CNTs or dark brown–purple SbSeI@CNTs sols were obtained. The products were extracted using the MPW–223e centrifuge (MPW Med. Instruments, Poland). Liquids above sediments were replaced with pure alcohol to wash the precipitates. The centrifugation and washing were performed 5 times. Finally, alcohol was evaporated from the samples in air at room temperature.

Characterization of the CNTs filled with SbSI or SbSeI was accomplished using different techniques. Powder X-ray diffraction (XRD) was performed on JDX-7S X-ray diffractometer (JEOL, Japan) with graphite monochromatized Cu K_α radiation (λ = 0.154056 nm). Scanning electron microscopy (SEM) and energy dispersive X-ray spectroscopy (EDS) were done using STEM HD-2300A (Hitachi, Japan) with linescan EDS. High–resolution transmission electron microscopy (HRTEM) and selected area electron diffraction (SAED) were carried out on JEM 3010 microscope (JEOL, Japan).

The optical spectroscopy of thin films of SbSI@CNTs and SbSeI@CNTs deposited on BK-7 glass substrates was performed inside vacuum chamber containing two integrating spheres (Ocean Optics Inc., USA). One of them measured the light diffusely transmitted through the sample, while the second one (combined with light source) was used to determine the diffuse reflection spectra. The chamber was equipped with K2205 cryogenic microminiature refrigeration II-B system and K-77 temperature controller (MMR Technologies, Inc., USA). Vacuum inside the chamber was obtained using TSH 071E turbomolecular drag pumping station (Pfeiffer, Germany). The optical signals were measured with PC2000 (Ocean Optics Inc., USA) spectrophotometer. The spectral characteristics were registered using the OOI-Base program (Ocean Optics Inc., USA). The measurements were carried out in the temperature range from 274 K to 333 K.

Nanosensors were prepared using technique presented in [20]. Si/SiO_2 substrates equipped with Au electrodes separated by a gap of 1 μm were placed in TO-8 packages (TEC Microsystems, Germany). The electrical connections between gold electrodes on Si/SiO_2 substrate and pins on TO-8 package were made using HB05 thermosonic wire bonder (TPT Wire Bonder, Germany). The fabricated nanomaterials were dispersed in toluene using ultrasonic reactor IS-UZP-2 (InterSonic, Poland). DC electric field of $5 \cdot 10^5$ V/m was applied during the deposition of SbSI@CNTs or SbSeI@CNTs sol to align the nanotubes perpendicularly to electrodes. The number of the nanotubes bridging electrodes was controlled by their concentration in sol. It was possible to deposit a few nanotubes upon one substrate. Toluene was evaporated from samples at room temperature in glove box 830-ABC/EXP (Plas-Labs Products, USA).

In the next step of nanodevice fabrication, ultrasonic bonding technique was used to connect SbSI@CNTs or SbSeI@CNTs with Au microelectrodes. It was done using ultrasonic generator ADG70-100P-230-NO (Rinco Ultrasonics, Switzerland) equipped with transducer C 70-2 (working frequency 70 kHz, max power 120 W) and homemade sonotrode ended with single crystal silicon carbide (SiC) head [20]. Ultrasonic processing was carried out at room temperature, applying one ultrasonic impulse of 0.04(1) μm amplitude, 0.5(1) J energy and 90(4) ms duration. The clamping force of the welding head was 0.89(3) N.

Characterization of the fabricated nanotubes-Au bonds was performed using SEM and DC electrical investigations. Scanning electron micrographs were taken on Phenom Pro X microscope (Phenom World, Netherlands). The acceleration voltage was 10 kV. Electric investigations were done using a DC voltamperometric technique in ambient air at normal pressure. Electrometer 6517A and 6430 sub-femtoamp remote source-meter (Keithley, USA) were used. Acquisition of the data was realized using PC computer with GPIB bus and appropriate program in LabView (National Instruments, USA).

Gas sensing properties of SbSI@CNTs and SbSeI@CNTs were tested for carbon dioxide (CO_2). The experimental set up consisted of test chamber, TW70H turbomolecular vacuum pump (Prevac, Poland), vacuum gauge controller ACM 1000 with gauges ACC 1009, ADS 1001 and ADS 1004 (Alcatel, France), mass flow controllers SLA 5850 (Brooks Instruments, USA), thermostat HAAKE DC30 with kessel HAAKE K20 circulator (Thermo Scientific, USA), Pt-100 sensor with temperature controller Model 211 (Lake Shore, USA), and humidity sensor SHT15 (Sensirion AG, Switzerland) with humidity meter ES-1530 (Elektro-System, Poland). Before experiments with CO_2, nanosensors were held at 323 K temperature in vacuum (10^{-2} Pa) for 30 min. The DC electric investigations of gas sensors were performed using the mentioned above instruments.

3. Results and discussion

Dried gels of SbSI@CNTs and SbSeI@CNTs are composed of a large number of tangled CNTs (see Supporting Information, Fig. S1). The difference in colors of them is caused by energy gaps of SbSI and SbSeI. Fig. 1 shows temperature dependent spectral characteristics of diffusive reflectance $R_d(\lambda, T)$ and transmission $T_d(\lambda, T)$ of investigated materials. Knowing $R_d(\lambda, T)$ and $T_d(\lambda, T)$ one can determine spectra of the Kubelka-Munk scattering (S_{KM}) and absorbance (A_{KM}) coefficients for different temperatures [21]:

$$S_{KM} = \frac{1}{yw} \ln\left[\frac{1 - R_d(x-y)}{T_d}\right] \quad (1)$$

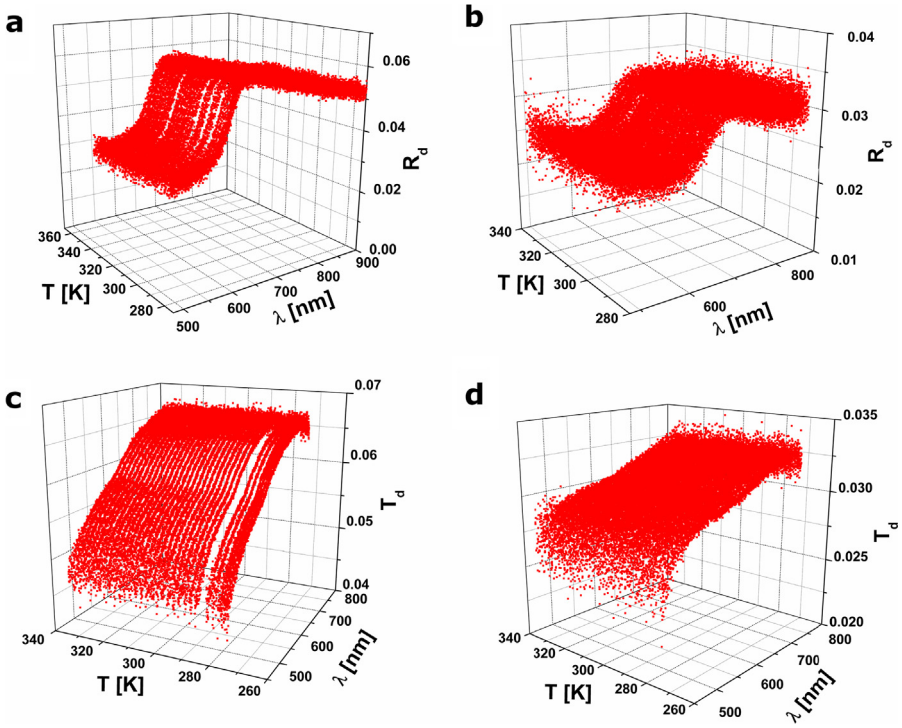

Fig. 1. Spectral characteristics of diffusive reflectance (a, b) and transmission (c, d) for SbSI@CNTs (a, c) and SbSeI@CNTs (b, d) at different temperatures.

$$A_{KM} = (x-1)S_{KM} \tag{2}$$

where w is sample thickness; parameters x and y are calculated using the following formulae:

$$x = \frac{1 + R_d^2 - T_d}{2R_d} \tag{3}$$

$$y = +\sqrt{x^2 - 1} \tag{4}$$

Fig. 2 shows spectral characteristics of scattering and absorbance coefficients for SbSI@CNTs and SbSeI@CNTs at one temperature. Applying simultaneous fitting [22] of many absorption mechanisms to the spectral dependence of A_{KM}, one can determine optical energy gap of investigated material. For SbSI@CNT the best fitting was obtained for the sum of indirect forbidden absorption without excitons and phonon statistics, free carrier absorption and constant absorption term associated with light scattering independent of the wavelength. The best fitting for SbSeI@CNT was obtained for the sum of indirect allowed absorption without phonon statistics and the constant absorption term. Energy gaps of SbSI@CNT and SbSeI@CNT decrease with increasing temperature (Fig. S2). Temperature dependences of indirect forbidden optical energy gap of SbSI@CNT and indirect allowed optical energy gap of SbSeI@CNT were fitted (Fig. S2) with $E_{gIf}(T) = 1.92(2)$ [eV] $- 3.6(6) \cdot 10^{-4} \cdot T$ [eV/K] and $E_{gIa}(T) = 1.817(5)$ [eV] $- 7.1(2) \cdot 10^{-4} \cdot T$ [eV/K], respectively.

The well-defined, sharp diffraction lines in powder XRD patterns of SbSI@CNT and SbSeI@CNT (Fig. S3) suggested the well-crystallized substances. In both cases, the diffraction lines were divided into three groups. The identification of them was done using PCSIWIN computer program and the data from JCPDS-International Centre for Diffraction Data 2000. In both cases, the first group of peaks was indexed to carbon phase $P6_3mc$ with the cell constants a = 0.2470 nm and c = 0.6790 nm [23]. The second group of a few additional X-ray diffraction lines was attributed to the monoclinic antimony iodide (SbI_3) with the cell constants

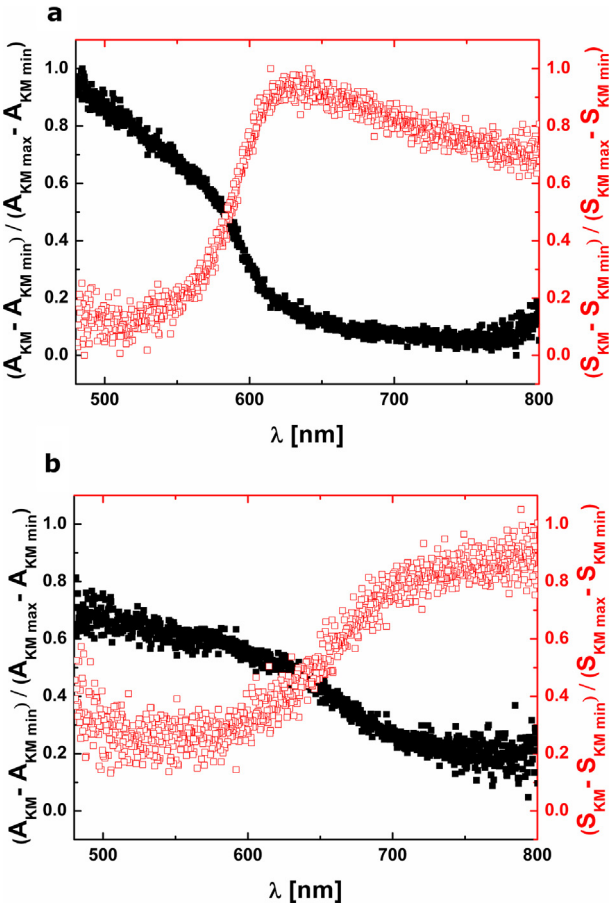

Fig. 2. Spectral characteristics of absorbance (■) and scattering (□) coefficients for SbSI@CNTs and SbSeI@CNTs at T = 274 K.

a = 0.7281 nm, b = 1.0902 nm, c = 0.8946 nm, and β = 109.930° [24]. In the case of SbSI@CNTs, the most numerous group of diffraction lines was indexed to pure orthorhombic phase of SbSI [25] with the cell constants a = 0.858 nm, b = 1.017 nm, and c = 0.414 nm (Fig. S3a). The most numerous group of SbSeI@CNTs diffraction lines (Fig. S3b) was indexed to pure orthorhombic phase of SbSeI [26] with the cell constants a = 0.8698 nm, b = 1.0412 nm, and c = 0.4127 nm.

The existence of SbI_3 in the investigated samples can be explained as follows. Iodine in alcohol reacts with Sb forming antimony iodide. This compound is soluble in alcohols [27]. When the alcohol evaporates, the SbI_3 crystallizes. It is probable that (despite the washing of SbSI@CNT and SbSeI@CNT) small amount of SbI_3 still exists in the product. This problem should be solved in the future.

The EDS analysis of SbSI@CNTs and SbSeI@CNTs was also done. The characteristic peaks for antimony, iodine, and sulfur or selenium were observed (Figs. S4 and S5). Fig. S5 presents line EDS analysis of chemical composition in direction perpendicular to two SbSeI@CNTs. One can see the good filling of CNTs with SbSeI. The elemental atomic ratios were equal 0.48(3):0.16(3):0.36(3) for Sb:S:I and 0.44(3):0.28(3):0.28(3) for Sb:Se:I, for SbSI and SbSeI in CNTs respectively (Table S1). They indicated nonstoichiometric SbSI and SbSeI that could be caused by formation of Sb-S-I and Sb-Se-I glasses [28,29]. However, it was improbable that the excess Sb was present within the ordered SbSI and SbSeI nanowires inside the CNTs, since the interplanar spacings corresponds to stoichiometric materials (Figs. 3 and 4). Therefore, probably separate phases of Sb and I (e.g. SbI_3 and Sb_3I [30]) were present in investigated samples. The existence of such phases in CNTs filled with Sb, I, and S or Se will be investigated in the future.

The TEM (Figs. 3a and 4a) and HRTEM images (Figs. 3b and 4b) of individual CNTs sonochemically filled with SbSI and SbSeI revealed that the products consist of coaxial nanocables. The lateral dimensions of SbSI@CNTs and SbSeI@CNTs were in the ranges from 30 nm to 200 nm and from 20 nm to 170 nm, respectively. Lengths of these nanocables reached up to several micrometers in both cases. The HRTEM and SAED investigations of SbSI@CNTs and SbSeI@CNTs (Figs. 3 and 4) proved the good crystallinity of the filling. The HRTEM image of individual CNT sonochemically filled with SbSI (Fig. 3b) exhibited its clear (220) lattice fringes parallel to the nanocable axis. It indicated the growth of SbSI inside the CNT in [001] direction. The interplanar spacing was 0.319(2) nm, which coincided with interplanar spacing 0.32494 nm of (220) planes of orthorhombic bulk SbSI [25]. Fig. 3b shows also the lattice fringes of the CNT walls. The fringe spacing of 0.209 (2) nm was in good agreement with the 0.21390 nm interplanar distances between (101) planes of carbon nanotubes [23]. All these results corresponded well with the XRD patterns (Fig. S3a) of CNTs sonochemically filled with SbSI. The SAED pattern (Fig. 3c) recorded at the end of CNT filled with SbSI (Fig. 3b) indicated interplanar spacings typical for CNTs as well as SbSI crystals (see Table 1).

The HRTEM image of an individual SbSeI@CNT (Fig. 4b) exhibited clear (200) lattice fringes of SbSeI parallel to the nanocable axis. It indicated the growth of SbSeI inside the CNT in [001] direction. The interplanar spacing was 0.432(13) nm, which coincided with the interplanar spacing 0.4349 nm for (200) planes of orthorhombic SbSeI [26]. Fig. 4b shows also the lattice fringes of CNT walls. The fringe spacing of 0.332(5) nm was in good agreement with the 0.3395 nm interplanar distances between (002) planes of carbon nanotubes [23]. All these results corresponded well with the XRD pattern (Fig. S3b) of CNTs sonochemically filled with SbSeI. The SAED pattern (Fig. 4c) of SbSeI@CNT (Fig. 4b) indicated the interplanar spacings characteristic for SbSeI crystals (Table 2).

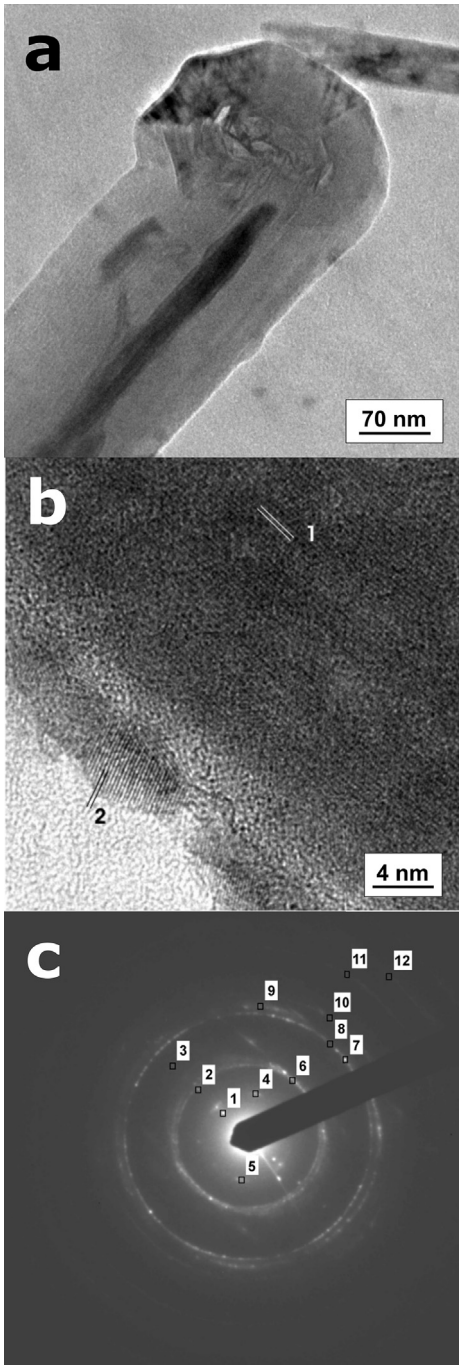

Fig. 3. Typical TEM (a) and HRTEM (b) images as well as electron diffraction pattern (c) of an individual SbSI@CNT (1–0.319(2) nm for (220) planes of SbSI crystal (b); 2–0.209(2) nm for (101) planes of carbon nanotube (b); description of SAED reflexes in Table 1).

Surprisingly, the presence of SbSI and SbSeI nanowires on the outer walls of CNTs was not observed in the HRTEM and TEM images. Probably, capillary suction of molecules into carbon nanotubes facilitated the process of SbSI and SbSeI nanocrystals growth.

It is known that the mode of insertion dictates the nature and morphology of the obtained filling of CNTs [31]. When the filling is induced via solution–deposition, small discrete encapsulates are formed, whereas when it is obtained via capillarity, continuously filled CNTs are observed. Probably the latter happens when CNTs are filled sonochemically by SbSI or SbSeI. The transient

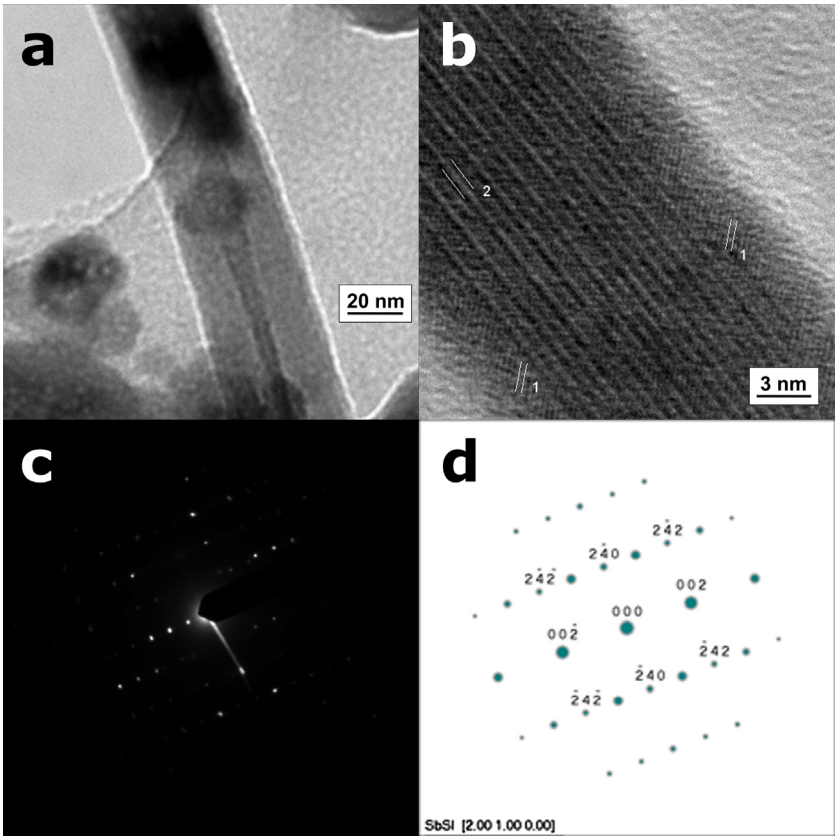

Fig. 4. Typical TEM (a) and HRTEM (b) images of an individual SbSeI@CNT as well as electron diffraction pattern (c) and its simulated diagram (d) (1–0.332(5) nm for (002) planes of carbon nanotube; 2–0.432(13) nm for (200) planes of SbSeI crystal; description of SAED reflexes in Table 2).

Table 1
Comparison of interplanar spacings determined by SAED (Fig. 3c) of SbSI@CNT with literature data for CNTs and SbSI bulk crystals.

Sign	Results of the SAED d_{hkl} (nm)	Literature data			
		for C [23]		for SbSI [25]	
		d_{hkl} (nm)	(hkl)	d_{hkl} (nm)	(hkl)
1 reflex	0.4360	–	–	0.43402	(120)
		–	–	0.42450	(200)
4 reflex	0.3732	–	–	0.38465	(011)
5 reflex	0.3470	0.33950	(002)	0.35036	(111)
2 reflex	0.2189	0.21390	(100)	0.21663	(330)
6	0.2089	0.20402	(101)	0.20800	(002)
3 reflex	0.1446	–	–	0.14244	(422)
		–	–	0.14244	(531)
7 reflex	0.1190	–	–	0.12031	(143)
		–	–	0.11960	(181)
8 circle	0.1210	0.12350	(110)	–	–
9 circle	0.1155	0.11606	(112)	–	–
		0.11464	(105)	–	–
		0.11316	(006)	–	–
10 circle	0.1036	0.10425	(202)	–	–
11 circle	0.07874	0.07954	(122)	–	–
12 circle	0.07038	0.07720	(206)	–	–

high–temperature and high-pressure field produced during ultrasound irradiation provide a favorable environment for the 1D growth of SbSI [16] and SbSeI [32] nanocrystals from elements inside CNTs in alcohol, though the surrounding solution is at relatively low temperature (T = 323 K) and atmospheric pressure.

Simplified growth of SbSI-type materials in CNT is shown in Fig. 5. The probable reaction routes of SbSI and SbSeI synthesis in CNTs, and the mechanisms of nanowires formation using elemental Sb, S or Se and I_2 in the presence of methanol and/or ethanol under ultrasonic irradiation can be summarized as follows:

(a) iodine, I_2, dissolved in methanol or ethanol reacts with antimony and forms the antimony triiodide, SbI_3, also dissolved in alcohol [27]

$$2Sb + 3I_2 \rightarrow 2SbI_3 \quad (5)$$

Table 2
Comparison of interplanar spacings determined by SAED and HRTEM of SbSeI@CNT (Fig. 4) with literature data for CNTs and orthorhombic SbSeI crystals.

SAED		HRTEM		Literature data			
				C [23]		SbSeI [26]	
d_{hkl} [pm]	hkl	sign	d_{hkl} [pm]	d_{hkl} [pm]	hkl	d_{hkl} [pm]	hkl
		2	432(13)			434.9	200
		1	332(5)	339.5	002		
223.35	$2\bar{4}0$					223.35	240
206.35	002			204.02	101	206.35	002
151.56	$\bar{2}42$					151.56	242

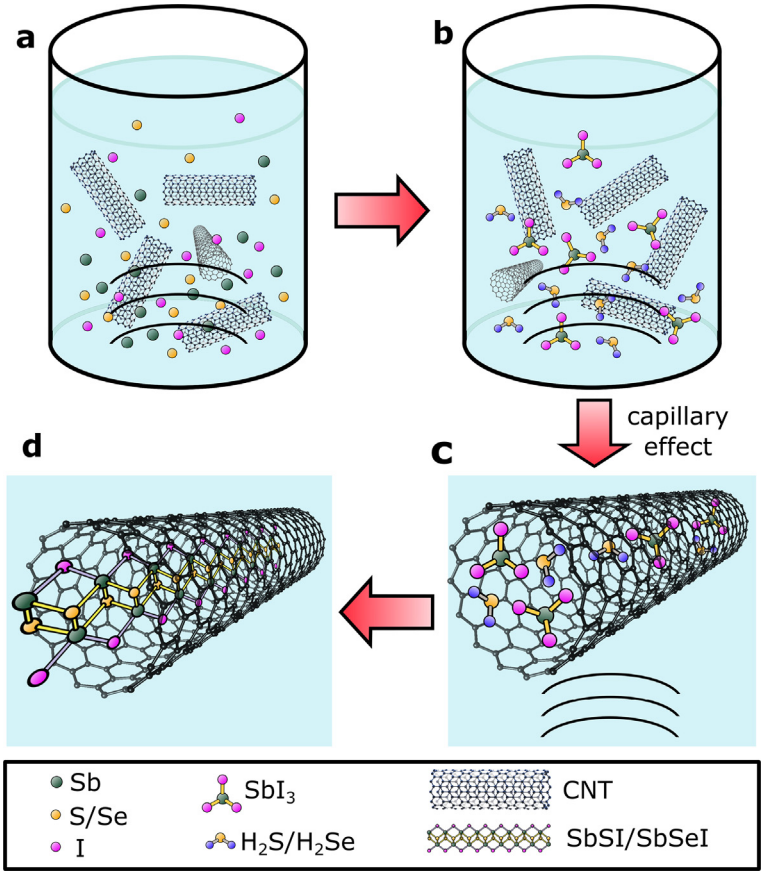

Fig. 5. Simplified growth of SbSI-type materials in CNT.

(b) dehydrogenation, dehydration as well as decomposition of ethanol and methanol in or close to the cavitation bubbles leads to the formation of water and hydrogen as well as the H· and OH· radicals [33];
(c) the sonolysis of water yields the H· and OH· radicals

$$H_2O \xrightarrow{)))} H^{\cdot} + OH^{\cdot} \quad (6)$$

(d) the ultrasonic irradiation facilitates the reduction of chalcogens to the active forms of S^{-2} and Se^{-2} (see Refs. in [11]) that react with the in-situ generated H· radicals forming H_2S and H_2Se [34]

$$S + 2H^{\cdot} \rightarrow H_2S \quad (7)$$

$$Se + 2H^{\cdot} \rightarrow H_2Se \quad (8)$$

(e) opening of the CNT ends can be affected due to presence of the acids (H_2S, H_2Se) [5] or the action of ultrasounds [35];
(f) CNTs suck the released H_2S or H_2Se molecules and SbI_3 in alkohol needed to build SbSI and SbSeI. This is allowed by the capillary effect [15]. It is well known [36,37], that open CNTs are impregnated with excess of the precursor solutions under ultrasonic conditions. From the thermodynamic point of view, the dissolution of the impregnating solution sticking to external walls of CNTs into the washing medium necessitates the condition of the solvation energy gain smaller than zero [36,37]. On the other hand, the energy gain for the capillary filling of a CNT must be smaller than the solvation energy to ensure that the solution is stable in the internal cavity of CNTs [36,37];
(g) H_2S or H_2Se reacts with SbI_3 to yield SbSI and SbSeI molecules

$$SbI_3 + H_2S \rightarrow SbSI + H_2 + I_2 \quad (9)$$

$$SbI_3 + H_2Se \rightarrow SbSeI + H_2 + I_2 \quad (10)$$

(h) SbSI or SbSeI molecules, under the microjets and shock-waves formed during collapse of the bubbles, are pushed towards each other in CNTs and are held by chemical forces. Therefore, the nuclei of SbSI or SbSeI are formed as a result of the interparticle collisions [11];
(i) the freshly formed nuclei in the solution are unstable and have the tendency to grow into double chains $[(SbSI)_{\infty}]_2$ or $[(SbSeI)_{\infty}]_2$ consisting of two chains related by a twofold screw axis and linked together by a short and strong Sb-S or Sb-Se bonds [38]. Local turbulent flow associated with cavitation and acoustic streaming greatly accelerates mass transport in the liquid phase;
(j) SbSI and SbSeI chains can be readily crystallized into a 3D lattice in the CNTs through van der Waals interactions. Induced by this structure, crystallization occurs along the c-axis, favoring the stronger covalent bonds over the relatively weak, inter-chain van der Waals forces [39]. Thus, this solid material has a tendency to form highly anisotropic, 1D structures also inside the CNTs.

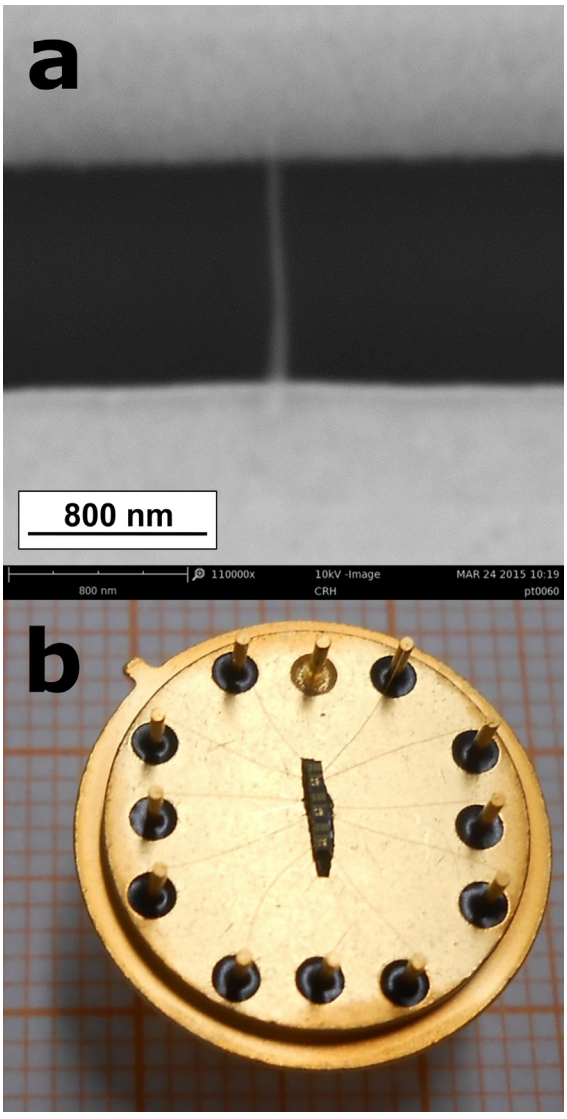

Fig. 6. SEM micrograph of single SbSI@CNT bonded ultrasonically to Au microelectrodes on Si/SiO_2 substrate (a) and image of SbSI@CNTs gas sensors mounted on TO-8 package (b).

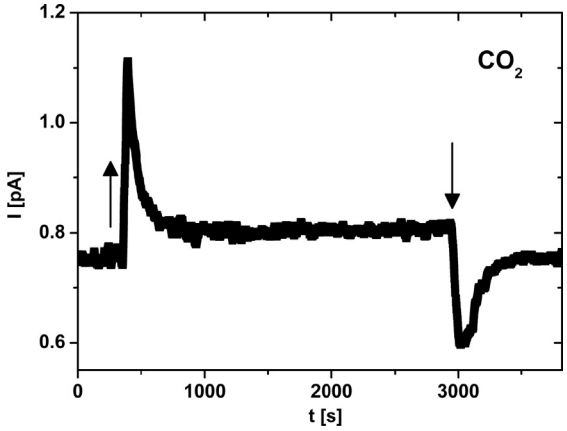

Fig. 7. Electric current response of SbSI@CNT on injection (↑) and ejection (↓) of CO_2 gas (p = 65 kPa; E = 10^6 V/m; T = 298 K).

The (9) and (10) were the basic reactions used in different methods of preparation of bulk SbSI-type crystals [40]. Despite the tubes filling, the observed nanowire type morphology of the product (Figs. 3 and 4) is possible due to the inherent chain type structure and growth habit of SbSI as well as SbSeI crystals [38].

Fig. 6 shows typical SEM image of an individual SbSI@CNT bridging two Au microelectrodes on Si/SiO_2 substrate after ultrasonic processing. Embedding the ends of SbSI@CNT into the metal one decreased two times the resistance of the sample (despite the fact that some of nanotubes were swept away from processed area during the action of ultrasound). It can be attributed to important fall of the contact resistance between Au microelectrodes and nanotubes.

To show the potential applicability of SbSI@CNTs as gas sensors, their transient response and recovery characteristics are presented in Fig. 7. It should be noted that recovery of sensor was simply realized by evacuation of gas from the test chamber. No heating of sensor was needed for desorption of CO_2 from SbSI@CNT surface. When CO_2 is introduced to test chamber, the electric current increases fast, attains maximum, and then decreases with time to a stationary value about few percent greater than the value of current in vacuum. When CO_2 is evacuated from chamber, the electric current decreases, reaches minimum and afterward increases to the initial level. The quick increase followed by a decrease of electric current after gas injection and quick decrease followed by an increase of electric current after gas removal can be related to the shock front propagation through the ferroelectric sample thickness [41,42]. Its mechanism is usually recognized as the effect of depolarization of ferroelectric element [41,43].

Carbon dioxide molecule is usually regarded as an electron acceptor [44]. It means that CO_2 adsorption at a semiconductor surface involves electron transfer from a semiconductor into the CO_2 molecule. It leads to the formation of a partially charged species $CO_2^{\delta-}$ through interactions with surface atoms [44]. For p-type SbSI [45], formation of $CO_2^{\delta-}$ ions enhances number of holes in the valence band, resulting in the increase of electric conductance.

4. Conclusions

Application of ultrasounds opens interesting possibilities in constructing nanodevices based on carbon nanotubes. The main advantages of the presented sonochemical filling of CNTs with SbSI or SbSeI nanophase are as follows. The synthesis can be performed at low temperature (e.g. at 323 K). It provides a convenient, fast, and mild route for producing hybrid nanomaterials. Probably this approach can be extended to the preparation of some other ternary

and quaternary nanomaterials formed from the group 15-16-17 elements within CNTs, e.g. $SbS_{1-x}Se_xI$@CNTs.

After DC electric field alignment of CNTs filled with ferroelectrics (e.g. SbSI and SbSeI), ultrasonic bonding technique can be successfully applied for joining of them with metal microelectrodes. It meets the important need of simply and convenient method to build reliable electrical interconnections at the nanoscale. Ultrasonic processing has caused 200% increase of DC electric conductance of the junctions between Au microelectrodes and SbSI@CNT and SbSeI@CNTs (despite the fact that some of nanotubes were swept away from processed area during the action of ultrasound).

One predicts that upscaling of the presented ultrasonic technologies (CNTs filling and bonding) will lead to large quantities of nanodevices containing chalcohalides encapsulated in CNTs. The understudy method of constructing novel SbSI@CNTs and SbSeI@CNTs nanodevices is distinct from literature in terms of its higher efficiency, simplicity, cost-effectiveness without using toxic and expensive reactants.

Electronic and optical properties of SbSI@CNTs and SbSeI@CNTs are considerably modified with respect to the CNTs. In the temperature range from 274 K to 333 K the optical energy gaps of SbSI@CNT and SbSeI@CNT are described by $E_{gIf}(T) = 1.92(2)\ [eV] - 3.6(6) \cdot 10^{-4} \cdot T\ [eV/K]$ and $E_{gIa}(T) = 1.817(5)\ [eV] - 7.1(2) \cdot 10^{-4} \cdot T\ [eV/K]$, respectively. One predicts that energy gap and other physical properties of carbon nanotubes filled with quaternary nanowires (e.g. $SbS_{1-x}Se_xI$@CNTs) should be tailored with stoichiometric composition.

Obviously, the new materials as the other one-dimensional nanostructures should receive considerable attention from the scientific and engineering communities due to their potentially useful electronic properties. One of the possible applications of the filled carbon nanotubes is their use as gas sensors. For the first time SbSI@CNTs structures have been successfully applied to detect carbon dioxide.

Acknowledgements

This paper was partially supported by the Institute of Physics - Center for Science and Education, Silesian University of Technology and financial support for young scientists (BK-243/RIF/2016, BKM-500/RIF/2016, BKM-502/RIF/2016, BK/RIF/2017, BKM/RIF/2017).

Appendix A. Supplementary material

Supplementary data associated with this article can be found, in the online version, at http://dx.doi.org/10.1016/j.ultras.2017.03.014.

References

[1] S. Iijima, Helical microtubules of graphitic carbon, Nature 354 (1991) 56–58, http://dx.doi.org/10.1038/354056a0.
[2] P.M. Ajayan, S. Iijima, Capillarity-induced filling of carbon nanotubes, Nature 361 (1993) 333–334, http://dx.doi.org/10.1038/361333a0.
[3] M. Monthioux, Filling single-wall carbon nanotubes, Carbon 40 (2002) 1809–1823, http://dx.doi.org/10.1016/S0008-6223(02)00102-1.
[4] Eduard G. Rakov, Chemistry of Carbon Nanotubes, in: Nanomaterials Handbook, Taylor & Francis Group, LLC, 2006, http://dx.doi.org/10.1201/9781420004014.ch5 (Chapter 5).
[5] A. Eliseev, L. Yashina, M. Kharlamova, N. Kiselev, One-dimensional crystals inside single-walled carbon nanotubes: growth, structure and electronic properties, in: J.M. Marulanda (Ed.), Electronic Properties of Carbon Nanotubes, InTech, Rijeka, 2011, pp. 127–156, http://dx.doi.org/10.5772/19060.
[6] P. Lukanov, C.-M. Tîlmaciu, A.M. Galibert, B. Soula, E. Flahaut, Filling of carbon nanotubes with compounds in solution or melted phase, in: R. Klingeler, R.B. Sim (Eds.), Carbon Nanotubes for Biomedical Applications, Carbon Nanostructures, Springer-Verlag, Berlin, 2011, http://dx.doi.org/10.1007/978-3-642-14802-6.
[7] M. Nowak, M. Jesionek, P. Szperlich, J. Szala, T. Rzychoń, D. Stróż, Sonochemical growth of antimony sulfoiodide in multiwalled carbon nanotube, Ultrason. Sonochem. 16 (2009) 800–804, http://dx.doi.org/10.1016/j.ultsonch.2009.03.007.
[8] M. Jesionek, M. Nowak, P. Szperlich, D. Stróż, J. Szala, K. Jesionek, T. Rzychoń, Sonochemical growth of antimony selenoiodide in multiwalled carbon nanotube, Ultrason. Sonochem. 19 (2012) 179–185, http://dx.doi.org/10.1016/j.ultsonch.2011.06.006.
[9] K.S. Suslick, G.J. Price, Applications of ultrasound to materials chemistry, Annu. Rev. Mater. Sci. 29 (1999) 295–326, http://dx.doi.org/10.1146/annurev.matsci.29.1.295.
[10] T.J. Mason, Sonochemistry and sonoprocessing: the link, the trends and (probably) the future, Ultrason. Sonochem. 10 (2003) 175–179, http://dx.doi.org/10.1016/S1350-4177(03)00086-5.
[11] A. Gedanken, Using sonochemistry for the fabrication of nanomaterials, Ultrason. Sonochem. 11 (2004) 47–55, http://dx.doi.org/10.1016/j.ultsonch.2004.01.037.
[12] G. Cravotto, P. Cintas, Power ultrasound in organic synthesis: moving cavitational chemistry from academia to innovative and large-scale applications, Chem. Soc. Rev. 35 (2006) 180–196, http://dx.doi.org/10.1039/B503848K.
[13] F. Nasiri Azad, M. Ghaedi, K. Dashtian, S. Hajati, V. Pezeshkpour, Ultrasonically assisted hydrothermal synthesis of activated carbon–HKUST-1-MOF hybrid for efficient simultaneous ultrasound-assisted removal of ternary organic dyes and antibacterial investigation: Taguchi optimization, Ultrason. Sonochem. 31 (2016) 383–393, http://dx.doi.org/10.1016/j.ultsonch.2016.01.024.
[14] P.S. Ardekani, Ha Karimi, M. Ghaedi, A. Asfaram, M.K. Purkait, Ultrasonic assisted removal of methylene blue on ultrasonically synthesized zinc hydroxide nanoparticles on activated carbon prepared from wood of cherry tree: experimental design methodology and artificial neural network, J. Mol. Liq. 229 (2017) 114–124, http://dx.doi.org/10.1016/j.molliq.2016.12.028.
[15] A.V. Eletskii, Sorption properties of carbon nanostructures, Physics-Uspekhi 47 (2004) 1119–1154, http://dx.doi.org/10.1070/PU2004v047n11ABEH002017.
[16] M. Nowak, P. Szperlich, Ł. Bober, J. Szala, G. Moskal, D. Stróż, Sonochemical preparation of SbSI gel, Ultrason. Sonochem. 15 (2008) 709–716, http://dx.doi.org/10.1016/j.ultsonch.2007.09.003.
[17] P. Szperlich, M. Nowak, Ł. Bober, J. Szala, D. Stróż, Ferroelectric properties of ultrasonochemically prepared SbSI ethanogel, Ultrason. Sonochem. 16 (2009) 398–401, http://dx.doi.org/10.1016/j.ultsonch.2008.09.001.
[18] K. Hamano, T. Nakamura, Y. Ishibashi, T. Ooyane, Piezoelectric property of SbSI single crystal, J. Phys. Soc. Jpn. 20 (1965) 1886–1887, http://dx.doi.org/10.1143/JPSJ.20.1886.
[19] M. Nowak, P. Mroczek, P. Duka, A. Kidawa, P. Szperlich, A. Grabowski, J. Szala, G. Moskal, Using of textured polycrystalline SbSI in actuators, Sensors Actuat. A 150 (2009) 251–256, http://dx.doi.org/10.1016/j.sna.2009.01.005.
[20] K. Mistewicz, M. Nowak, R. Wrzalik, J. Śleziona, J. Wieczorek, A. Guiseppi-Elie, Ultrasonic processing of SbSI nanowires for their application to gas sensors, Ultrasonics 69 (2016) 67–73, http://dx.doi.org/10.1016/j.ultras.2016.04.004.
[21] Wai-Fung Cheong, S.A. Prahl, A.J. Welch, IEEE J. Quantum. Elect. 26 (1990) 2166, http://dx.doi.org/10.1109/3.64354.
[22] M. Nowak, B. Kauch, P. Szperlich, Determination of energy band gap of nanocrystalline SbSI using diffuse reflectance spectroscopy, Rev. Sci. Instrum. 80 (2009) 046107, http://dx.doi.org/10.1063/1.3103603.
[23] Carbon, JCPDS-International Centre for Diffraction Data 2000, PCPDFWIN v. 2.1, Card File No. 75-1621.
[24] Antimony Iodide, JCPDS–International Centre for Diffraction Data 2000, PCPDFWIN v. 2.1, Card File No. 75-1417.
[25] Antimony Sulfide Iodide, JCPDS-International Centre for Diffraction Data 2000, PCPDFWIN v. 2.1, Card File No. 74-0149.
[26] Antimony Selenide Iodide, JCPDS–International Centre for Diffraction Data 2000, PCPDFWIN v. 2.1, Card File No. 76-1354.
[27] R.F. Rolsten, Iodide Metals and Metal Iodides, Wiley, New York, 1961.
[28] D. Savytskii, B. Knorr, V. Dierolf, H. Jain, Formation of laser-induced SbSI single crystal architecture in Sb–S–I glasses, J. Non-Cryst. Solids 377 (2013) 245–249, http://dx.doi.org/10.1016/j.jnoncrysol.2013.01.018.
[29] D. Savytskii, B. Knorr, V. Dierolf, H. Jain, Laser-induced growth of oriented Sb_2S_3 single crystal dots on the surface of $82SbSI–18Sb_2S_3$ glasses, J. Non-Cryst. Solids 431 (2016) 36–40, http://dx.doi.org/10.1016/j.jnoncrysol.2015.03.007.
[30] M. Nowak, P. Szperlich, E. Talik, J. Szala, T. Rzychoń, D. Stróż, A. Nowrot, B. Solecka, Sonochemical preparation of antimony subiodide, Ultrason. Sonochem. 17 (2010) 219–227, http://dx.doi.org/10.1016/j.ultsonch.2009.05.016.
[31] J. Sloan, J. Cook, A. Chu, M. Zwiefka-Sibley, M.L.H. Green, J.L. Hutchison, Selective deposition of UCl_4 and $(KCl)_x(UCl_4)y$ inside carbon nanotubes using eutectic and noneutectic mixtures of UCl_4 with KCl, J. Solid State Chem. 140 (1998) 83–90, http://dx.doi.org/10.1006/jssc.1998.7863.
[32] M. Nowak, B. Kauch, P. Szperlich, M. Jesionek, M. Kępińska, Ł. Bober, J. Szala, G. Moskal, T. Rzychoń, D. Stróż, Sonochemical preparation of SbSeI gel, Ultrason. Sonochem. 16 (2009) 546–551, http://dx.doi.org/10.1016/j.ultsonch.2009.01.003.
[33] Y. Mizukoshi, H. Nakamura, H. Bandow, Y. Maeda, Y. Nagata, Sonolysis of organic liquid: effect of vapour pressure and evaporation rate, Ultrason. Sonochem. 6 (1999) 203–209, http://dx.doi.org/10.1016/S1350-4177(99)00012-7.
[34] H.-L. Li, Y.-C. Zhu, S.-G. Chen, O. Palchik, J.-P. Xiong, Yu. Koltypin, Y. Gofer, A. Gedanken, A novel ultrasound-assisted approach to the synthesis of CdSe and

CdS nanoparticles, J. Sol. State Chem. 172 (2003) 102–110, http://dx.doi.org/10.1016/S0022-4596(02)00138-X.
[35] Chunwei Yang, Xinguo Hu, Dianlong Wang, Changsong Dai, Liang Zhang, Haibo Jin, Simeon Agathopoulos, Ultrasonically treated multi-walled carbon nanotubes (MWCNTs) as PtRu catalyst supports for methanol electrooxidation, J. Power Sources 160 (2006) 187–193, http://dx.doi.org/10.1016/j.jpowsour.2006.05.015.
[36] F.U. Qiang, G. Weinberg, S.U. Dang-sheng, Selective filling of carbon nanotubes with metals by selective washing, New Carbon Mater. 23 (2008) 17–20, http://dx.doi.org/10.1016/S1872-5805(08)60008-6.
[37] P.G. De Gennes, F. Brochard-Wyart, D. Quere, Capillarity and Wetting Phenomena: Drops, Bubbles, Pearls, Waves, Springer, Berlin, 2003, http://dx.doi.org/10.1007/978-0-387-21656-0.
[38] G.P. Voutsas, P.J. Rentzeperis, The crystal structure of the quaternary compound SbSe0.75S0.25I, Z. Kristallogr. 178 (1986) 289–295, http://dx.doi.org/10.1524/zkri.1987.178.14.289.
[39] B. Molnar, R. Johannes, W. Haas, Properties of single-crystal SbSI, Bull. Am. Phys. Soc. 10 (1965) 109.
[40] E.I. Gerzanich, V.A. Lyakhovitskaya, V.M. Fridkin, B.A. Popovkin, SbSI and other ferroelectric AVBVICVII materials, in: E. Kaldis (Ed.), Current Topics in Materials Science, 10, North-Holland, Amsterdam, 1982, pp. 55–190, http://dx.doi.org/10.1002/crat.2170190307.
[41] S.I. Shkuratov, E.F. Talantsev, J. Baird, Application of piezoelectric ceramics in pulsed power technology and engineering, in: E. Suaste-Gomez (Ed.), Piezoelectric Ceramics, Sciyo, Croatia, 2010, pp. 269–294, http://dx.doi.org/10.5772/9949.
[42] K. Mistewicz, M. Nowak, D. Stróż, R. Paszkiewicz, SbSI nanowires for ferroelectric generators operating under shock pressure, Mater. Lett. 180 (2016) 15–18, http://dx.doi.org/10.1016/j.matlet.2016.05.093.
[43] L.L. Altgilbers, J. Baird, B.L. Freeman, C.S. Lynch, S.I. Shkuratov, Explosive Pulsed Power, Imperial College Press, London, 2011, http://dx.doi.org/10.1142/9781848163232.
[44] S.N. Habisreutinger, L. Schmidt-Mende, J.K. Stolarczyk, Photocatalytic reduction of CO_2 on TiO_2 and other semiconductors, Angew. Chem. Int. Ed. Engl. 52 (2013) 7372–7408, http://dx.doi.org/10.1002/anie.201207199.
[45] K. Mistewicz, M. Nowak, A. Starczewska, M. Jesionek, T. Rzychoń, R. Wrzalik, A. Guiseppi-Elie, Determination of electrical conductivity type of SbSI nanowires, Mater. Lett. 182 (2016) 78–80, http://dx.doi.org/10.1016/j.matlet.2016.06.073.